Title

Ultrafast transient absorption spectra and kinetics of human blue cone visual pigment at room temperature.

Journal

Proceedings of the National Academy of Sciences, 121(41)

Authors

Krishnamoorthi, Arjun

Salom, David

Wu, Arum

et al.

Publication Date

2024-10-08

DOI

10.1073/pnas.2414037121

Peer reviewed

PNAS RESEARCH ARTICLE | APPLIED PHYSICAL SCIENCES BIOCHEMISTRY OPEN ACCESS

Ultrafast transient absorption spectra and kinetics of human blue cone visual pigment at room temperature

Arjun Krishnamoorthi[a], David Salom[b,c], Arum Wu[b,c], Krzysztof Palczewski[b,c,d,e,f], and Peter M. Rentzepis[a,1]

Contributed by Peter M. Rentzepis; received July 12, 2024; accepted September 1, 2024; reviewed by Ali Er and Dmitri Voronine

The ultrafast photochemical reaction mechanism, transient spectra, and transition kinetics of the human blue cone visual pigment have been recorded at room temperature. Ultrafast time-resolved absorption spectroscopy revealed the progressive formation and decay of several metastable photo-intermediates, corresponding to the Batho to Meta-II photo-intermediates previously observed with bovine rhodopsin and human green cone opsin, on the picosecond to millisecond timescales following pulsed excitation. The experimental data reveal several interesting similarities and differences between the photobleaching sequences of bovine rhodopsin, human green cone opsin, and human blue cone opsin. While Meta-II formation kinetics are comparable between bovine rhodopsin and blue cone opsin, the transition kinetics of earlier photo-intermediates and qualitative characteristics of the Meta-I to Meta-II transition are more similar for blue cone opsin and green cone opsin. Additionally, the blue cone photo-intermediate spectra exhibit a high degree of overlap with uniquely small spectral shifts. The observed variation in Meta-II formation kinetics between rod and cone visual pigments is explained based on key structural differences.

blue cone opsin | cone photo-intermediates | cone visual pigments | phototransduction | ultrafast spectroscopy

Significance

Vision is enabled by rod and cone photoreceptor cells, which contain distinct rod and cone visual pigments that operate under scotopic (dim light or twilight) and photopic (bright light or daylight) conditions, respectively. While the mechanism of rod visual pigment (rhodopsin) activation is thoroughly characterized, equivalent processes in cone visual pigments (cone opsins) are significantly less understood. In this study, we performed ultrafast time-resolved spectroscopic experiments on human blue cone opsin to elucidate its unique photochemical reaction mechanism. These results advance our knowledge about the activation of cone visual pigments, which mediate most of our vision.

Rods and cones are distinct types of photoreceptor cells that comprise the vertebrate retina and initiate the visual process (1–5). Rods are mostly concentrated in the peripheral retina, whereas the cones are highly concentrated in the central foveal region (6). While rods provide scotopic (dim light or twilight) vision with extremely high, single-photon sensitivity (7, 8), cones mediate photopic (bright light or daylight) vision that is characterized by comparatively lower sensitivity yet superior spatial, temporal, and spectral resolution (1, 2, 4–6, 9, 10). In humans, there is a single type of rod visual pigment (rhodopsin) with maximum absorption at ~498 nm that mediates scotopic vision, along with three distinct types of blue (~420 nm), green (~530 nm), and red (~560 nm) cone visual pigments (cone opsins) that enable trichromatic color vision (11–14). Consequently, cones could be considered the primary source of visual information, although there are ~20 times more rods than cones in the human retina (2, 3, 15).

Vision is initiated through the absorption of light by the rod and cone visual pigments that densely occupy the outer segment portions of the photoreceptor cells (6, 16). Rod and cone visual pigments are prototypical G protein-coupled receptors (GPCRs) that generally consist of an 11-*cis*-retinal chromophore covalently attached to an opsin protein through a protonated Schiff base linkage (9, 17–21). Structural differences among the various rod and cone opsins, which result in unique electrostatic interactions between the retinal and nearby amino acid residues situated in the chromophore binding pocket, lead to the distinct spectral responses of the rod and cone visual pigments (5, 11, 19, 22). Variations in the chromophore, which is 11-*cis*-retinal in most vertebrates (including humans), can also significantly shift the absorption maximum of the visual pigment (22–24).

The absorption of light by a visual pigment triggers the ultrafast isomerization of the retinal chromophore from an 11-*cis*- to an all-*trans*-configuration (9, 19, 25), which subsequently initiates a series of conformational changes in the opsin protein, resulting in the progressive formation and decay of several metastable photo-intermediates on the femtosecond to millisecond timescales (18, 19, 26–30). In rhodopsin, the G (guanine nucleotide-binding) protein-activating state known as metarhodopsin II (Meta-II), in which the all-*trans*-retinal chromophore is bound to the opsin protein through a deprotonated Schiff base linkage (19), activates an enzymatic signaling cascade that ultimately generates a visual electrical signal (4, 9, 10, 31). Several biochemical studies (3, 32, 33) have demonstrated that the general mechanisms of rod and cone phototransduction are largely the same, where the distinct functional properties of the rods and cones are significantly dictated by differences in the lifetime of Meta-II (34–37), in addition to the differing expression and activity levels of the rod and cone phototransduction proteins (3).

Author affiliations: [a]Department of Electrical and Computer Engineering, Texas A&M University, College Station, TX 77843; [b]Department of Ophthalmology, Gavin Herbert Eye Institute, University of California Irvine, Irvine, CA 92697; [c]Department of Ophthalmology, School of Medicine, University of California Irvine, Irvine, CA 92697; [d]Department of Chemistry, University of California Irvine, Irvine, CA 92697; [e]Department of Physiology and Biophysics, University of California Irvine, Irvine, CA 92697; and [f]Department of Molecular Biology and Biochemistry, University of California Irvine, Irvine, CA 92697

Author contributions: A.K. and P.M.R. designed research; A.K. performed research; D.S., A.W., and K.P. contributed new reagents/analytic tools; A.K. and P.M.R. analyzed data; and A.K. and P.M.R. wrote the paper.

Reviewers: A.O.E., Western Kentucky University; and D.V., University of South Florida.

The authors declare no competing interest.

[1]To whom correspondence may be addressed. Email: prentzepis@tamu.edu.

Published October 2, 2024.

Ultrafast time-resolved spectroscopic studies of the visual pigments, most prominently rhodopsin (27, 28, 38–40), have provided substantial knowledge regarding the transient molecular spectra, kinetics, and structures of the distinct photo-intermediate species formed on the femtosecond to millisecond timescales following photon absorption. Low-temperature (41–45) and room-temperature (26, 27, 46–53) time-resolved spectroscopic studies of rhodopsin have revealed the progressive formation and decay of the metastable bathorhodopsin (Batho), lumirhodopsin (Lumi), and metarhodopsin I/II (Meta-I/II) photo-intermediates following visual pigment excitation. Femtosecond spectroscopy has demonstrated that the 11-*cis*- to all-*trans*-retinal isomerization occurs within ~200 fsec (54) following photon absorption, resulting in the initial, short-lived reaction product photorhodopsin, which subsequently relaxes to bathorhodopsin within a few picoseconds (38–40, 47, 55). The subsequent Lumi, Meta-I, and Meta-II photo-intermediates have been recorded and characterized, with respect to both the photo-intermediate absorption difference (ΔOD) spectra and transition kinetics, on the nanosecond to millisecond timescales at room temperature (46, 56). In addition, it has been demonstrated that specific nanobodies can trap photoactivated rhodopsin in Lumi- or Meta-I-like conformations at room temperature, thus functioning as allosteric modulators (57). Such studies have provided a thorough description of the rhodopsin photobleaching sequence that results in Meta-II formation and subsequent G protein activation.

While the mechanism of rhodopsin activation is substantially characterized, the equivalent ultrafast to millisecond photoreaction mechanisms for cone visual pigments are virtually unknown, which is primarily due to the inherent difficulties in isolating and stabilizing sufficiently large amounts of pure cone opsins for pump–probe spectroscopic studies (11, 58, 59). As a result, very few of the existing time-resolved studies (33, 36, 37, 60–62) on cone visual pigments, especially human cone opsins, have been conducted on the submillisecond timescales. Hence, limited information exists about the cone opsin photo-intermediates formed prior to Meta-II. Picosecond and nanosecond laser photolysis studies (62–65) of iodopsin (chicken red cone opsin) demonstrated that the iodopsin photobleaching sequence is qualitatively similar to that of bovine rhodopsin, consisting of equivalent Batho, Lumi, and Meta-I/II photo-intermediates with generally faster reaction kinetics, in addition to a distinct "BL-intermediate" that is analogous to the "blue-shifted intermediate" (BSI) previously identified in the bovine rhodopsin photobleaching sequence (27, 41, 66, 67). Our recent ultrafast time-resolved absorption study (68) of the human green cone visual pigment similarly revealed a unique BL-intermediate formed on the nanosecond timescale, but in contrast to the iodopsin photobleaching sequence (62, 63, 65), the transition kinetics for all human green cone photo-intermediates were slower compared to those for bovine rhodopsin. In addition, we observed incomplete conversion of Meta-I to Meta-II for human green cone opsin but not for bovine rhodopsin. Consequently, substantial questions remain about cone pigment activation, including whether the BL-intermediate is conserved across the various cone visual pigments; how the transient photo-intermediate spectra and transition kinetics, in particular Meta-II formation kinetics, compare between the rod and cone visual pigments on the ultrafast to millisecond timescales; and whether the nature of the Meta-I to Meta-II transition differs between the rod and cone visual pigments. Such information would greatly enhance our understanding of cone-mediated vision, which is our primary form of vision yet significantly less understood.

In this study, we performed ultrafast transient absorption spectroscopy on the human blue cone visual pigment at room temperature to determine its photochemical reaction mechanism on the picosecond to millisecond timescales. Human blue cone opsin belongs to the short-wavelength sensitive, or SWS1, opsin gene class (9, 22, 69). Previous site-directed mutagenesis studies (70–72) of the human blue cone visual pigment have identified the specific amino acid residues that tune its ground-state absorption spectrum, which is blue-shifted relative to that of the free 11-*cis*-retinal protonated Schiff base (11), unlike bovine rhodopsin and the other human cone opsin pigments. Low-temperature spectroscopy of chicken blue cone opsin (73) suggested that a similar sequence of photo-intermediates as iodopsin forms following light irradiation. Our experimental data indicate that the transient absorption spectra and kinetics of the human blue cone opsin photo-intermediates share multiple similarities and differences with those of bovine rhodopsin and human green cone opsin. Additionally, several aspects of the blue cone opsin photobleaching sequence, with respect to the photo-intermediate ΔOD band maxima and corresponding spectral shifts, are highly unique. A structural mechanism is tentatively proposed to explain the observed kinetic differences in Meta-II formation between the rod and cone visual pigments.

Results

Picosecond to Nanosecond Transient Absorption Spectra and Kinetics. The picosecond to nanosecond time evolution of the ΔOD spectra for human blue cone opsin, following excitation with a picosecond optical pulse, is shown in Fig. 1. The ultrafast formation of a red-shifted (relative to the ground-state absorption band maximum) absorption band, with its corresponding ΔOD band maximum located at ~460 nm, is clearly observed at a pump–probe delay of 67 psec (Fig. 1*B*). We assign this ultrafast, red-shifted ΔOD band, which is practically formed within the picosecond pump pulse width, to the Batho-intermediate of human blue cone opsin. Subsequently, the Batho-intermediate ΔOD band gradually undergoes a redshift in its band maximum on the picosecond to nanosecond timescales, as shown in Fig. 1*B* through 1E, suggesting the transformation of the initial, metastable Batho-intermediate into a distinct species.

Comparison of the ΔOD spectra at pump–probe delay times of 67 psec and 2 nsec, as displayed in Fig. 2*A*, clearly demonstrates that the Batho-intermediate is converted into another distinct photo-intermediate with a ΔOD band maximum that is red-shifted by ~20 nm relative to the Batho-intermediate. The isosbestic point for this transition process is ~470 nm. We interpret this as representing the conversion of the initial Batho-intermediate into the subsequent BL-intermediate of human blue cone opsin within a few nanoseconds following pulsed excitation. We find that the BL-intermediate ΔOD band, in addition to being red-shifted, is relatively broader and more diffuse compared to that of the Batho-intermediate, which results in considerable overlap between the respective photo-intermediate ΔOD spectra. The ultrafast kinetics of the Batho to BL transition are plotted in Fig. 2*B* with an estimated time constant of ~0.5 nsec.

Nanosecond Transient Absorption Spectra and Kinetics. The nanosecond transient absorption spectra and kinetics of human blue cone opsin, following excitation with a nanosecond optical pulse, are shown in Figs. 3 and 4. The nanosecond time-resolved spectra from 4 nsec to 800 nsec, as displayed in Fig. 3, reveal the formation of the BL-intermediate within the nanosecond pump pulse width, whereupon the BL-intermediate gradually decays into another photo-intermediate with a blue-shifted ΔOD band maximum. We identify this blue-shifted intermediate as the

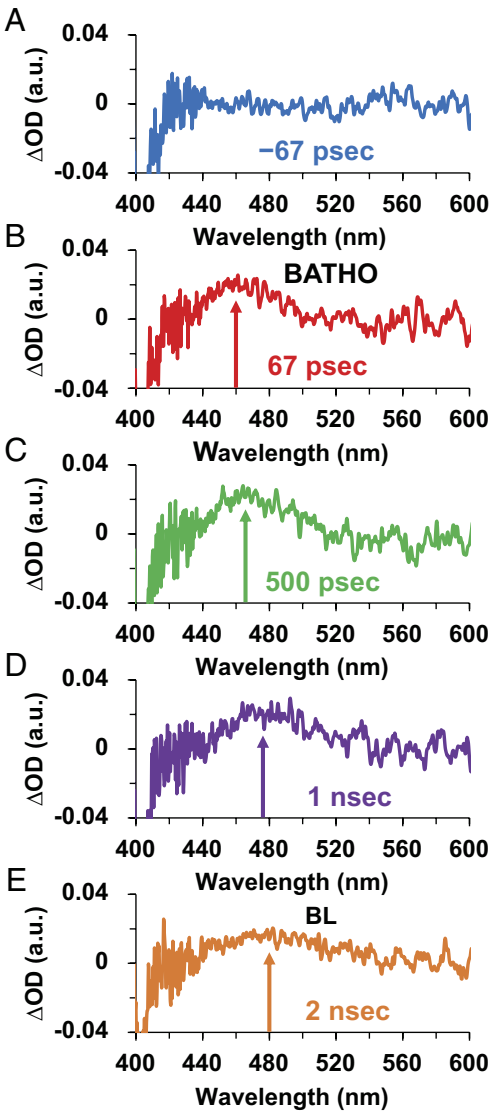

Fig. 1. Picosecond to nanosecond transient absorption spectra of human blue cone opsin at pump–probe delay times of (*A*) −67 psec, (*B*) 67 psec (Batho-intermediate), (*C*) 500 psec, (*D*) 1 nsec, and (*E*) 2 nsec (BL-intermediate). The arrow at each individual pump–probe delay time designates the approximate wavelength of the corresponding ΔOD band maximum. Note the progressive redshift of the ΔOD band maximum with increasing pump–probe delay time.

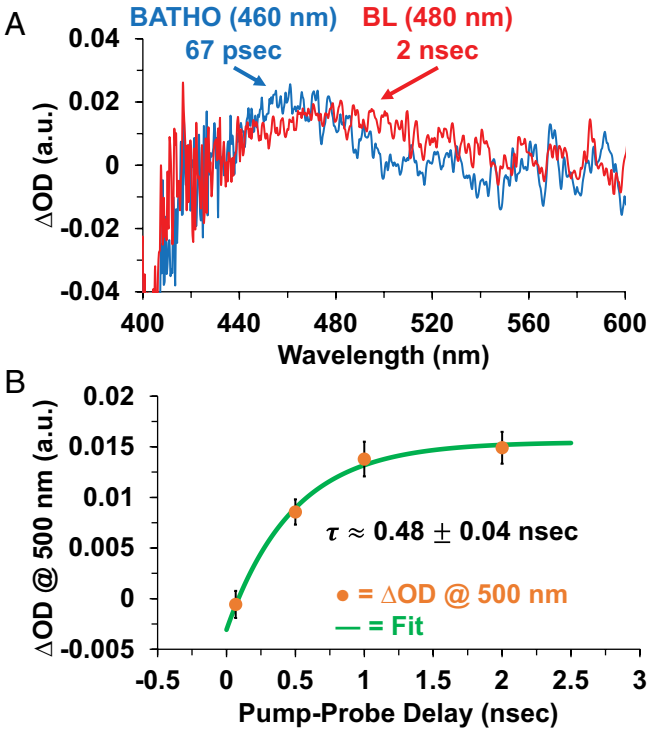

Fig. 2. Picosecond to nanosecond transient absorption spectra and kinetics of human blue cone opsin. (*A*) Picosecond to nanosecond transient absorption spectra at pump–probe delay times of 67 psec (blue) and 2 nsec (red), demonstrating the conversion of the Batho-intermediate into a distinct BL-intermediate for human blue cone opsin. The approximate ΔOD band maxima of the photo-intermediates are noted. (*B*) Corresponding picosecond formation kinetics for the BL-intermediate based on the increase in the average ΔOD at ~500 nm. Each individual data point corresponds to the average ΔOD value computed across several pump laser shots at a given pump–probe delay time, and the error bars at each data point represent one SD from the mean.

Lumi-intermediate of human blue cone opsin, where the Lumi-intermediate has an ~20 nm blue-shifted ΔOD band maximum relative to that of the BL-intermediate.

The corresponding BL-intermediate and Lumi-intermediate ΔOD spectra at pump–probe delay times of 4 nsec and 800 nsec (Fig. 4*A*), respectively, appear to be highly overlapped in the ~460 to 500 nm spectral range with an isosbestic point of ~465 nm for this transition process. The kinetics of the BL to Lumi transition are estimated based on the ΔOD kinetic trace recorded at a probe wavelength of 450 nm, corresponding to the progressive formation of the Lumi-intermediate, which is well fitted by a single-exponential model with an associated time constant of ~317 nsec (Fig. 4*B*). At probe wavelengths located near the BL-intermediate ΔOD band maximum at ~480 nm, as shown in Fig. 4*C*, we observed that the corresponding ΔOD kinetic traces were comparatively more complex and consisted of an initial, relatively rapid decay component (within the first ~50 to 100 nsec after pulsed excitation) followed by a secondary, substantially slower formation signal that persisted over the experimental timescale. A two-term exponential model was found to fit these kinetic traces reasonably well (Fig. 4*C*).

We attribute these observations to the fact that the BL-intermediate and Lumi-intermediate ΔOD bands are highly overlapped in this spectral region, where the decay of the BL-intermediate and concomitant formation of the Lumi-intermediate result in a net ΔOD signal that is not described by a single-exponential model and hence cannot be assigned to a single species. Due to the significant overlap between the BL-intermediate and Lumi-intermediate ΔOD spectra,

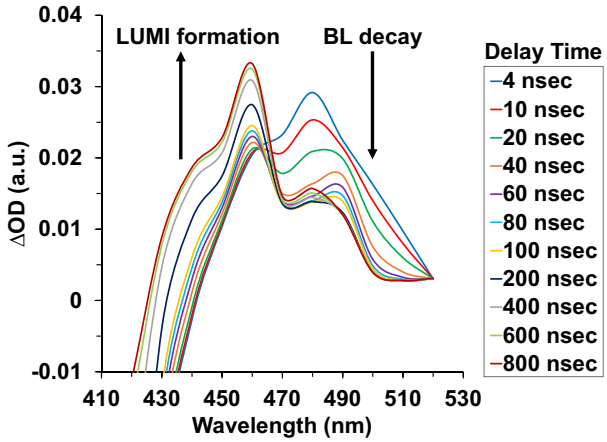

Fig. 3. Nanosecond transient absorption spectra of human blue cone opsin, illustrating the decay of the BL-intermediate and formation of the Lumi-intermediate on the nanosecond timescale. The spectra at each pump–probe delay time are computed based on the exponential fittings of the ΔOD kinetic traces at each recorded probe wavelength.

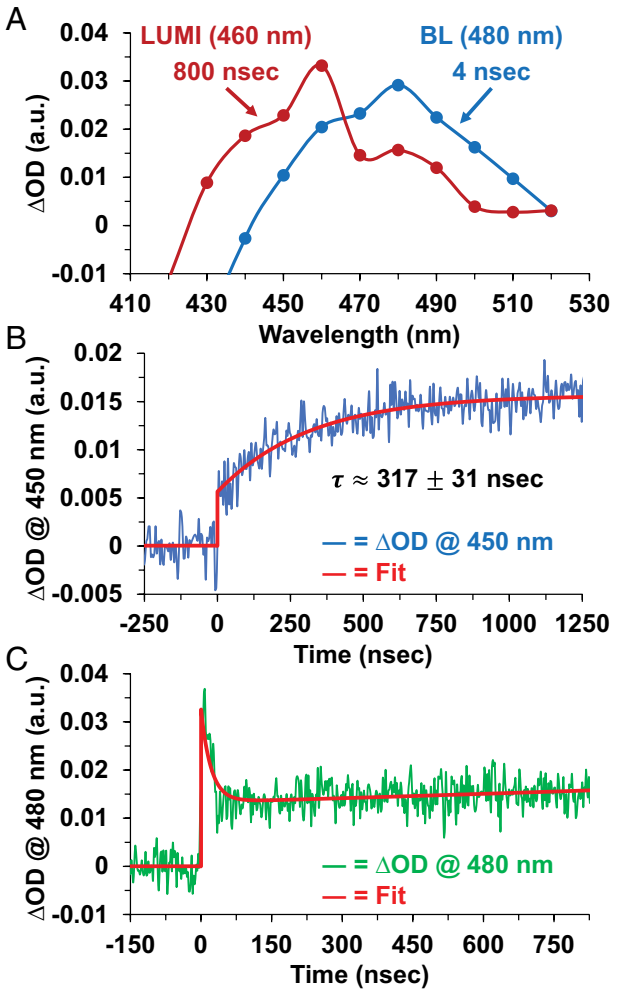

Fig. 4. Nanosecond transient absorption spectra and kinetics of human blue cone opsin. (*A*) Nanosecond transient absorption spectra of human blue cone opsin at pump–probe delay times of 4 nsec (blue) and 800 nsec (red), which are assigned to the BL-intermediate and Lumi-intermediate, respectively. The approximate ΔOD band maxima of the photo-intermediates are noted. (*B*) Nanosecond kinetic trace recorded at a probe wavelength of 450 nm, corresponding to the formation kinetics of the Lumi-intermediate. (*C*) Nanosecond kinetic trace recorded at a probe wavelength of 480 nm, demonstrating the considerable overlap in the BL-intermediate and Lumi-intermediate ΔOD spectra.

particularly in the spectral region of the BL-intermediate ΔOD band maximum, we were unable to directly record the decay kinetics of the BL-intermediate. Our recent time-resolved studies (46, 56, 68) at room temperature on bovine rhodopsin and human green cone opsin have demonstrated that the Batho/BL-intermediate decay and Lumi-intermediate formation in such visual pigments are single-transition processes with equivalent kinetics (within the experimental error). Therefore, we consider the recorded Lumi-intermediate formation kinetics (Fig. 4*B*), with an ~317 nsec time constant, to be a reasonable estimate of the BL to Lumi transition kinetics.

Microsecond to Millisecond Transient Absorption Spectra and Kinetics. The Fig. 5 displays the microsecond to millisecond transient absorption spectra and kinetics of human blue cone opsin after excitation with a nanosecond optical pulse. Following the formation of the Lumi-intermediate within a few microseconds after pulsed excitation, the ~455 nm ΔOD band maximum for the Lumi-intermediate subsequently decays and displays a progressive redshift in the ΔOD band maximum over the 2 μsec to 100 μsec timescale (Fig. 5*A*). After 100 μsec, the ΔOD band maximum has decreased by a factor of ~2.25 in magnitude with a slight, ~10 nm, redshift in the peak wavelength. We interpret this transition to represent the conversion of the Lumi-intermediate into the Meta-I intermediate of human blue cone opsin. This interpretation is substantiated by the fact that, over this same timescale, no appreciable increase in the ΔOD spectrum was observed in the ~350 to 400 nm spectral region, where the Meta-II intermediate of human blue cone opsin displays its ΔOD band maximum following photolysis (74), suggesting that the Lumi-intermediate must be transforming into a precursor of Meta-II. The Lumi-intermediate and Meta-I intermediate ΔOD spectra appear highly overlapped, and an isosbestic point of ~470 nm for this transition is visible only ~50 to 75 μsec after excitation, as shown in Fig. 5*A*, which is likely due to the sufficiently large decay of the Lumi-intermediate. The kinetics of the Lumi to Meta-I transition are estimated based on the decrease in ΔOD at a probe wavelength of ~440 nm, which is primarily due to the Lumi-intermediate decay and relatively unaffected by the formation of the Meta-I intermediate. Thus, this probe wavelength was selected to minimize the effect of the considerable overlap in the Lumi-intermediate and Meta-I intermediate ΔOD spectra. As shown in Fig. 5*B*, a time constant of ~48 μsec was computed for this transition. Fitting the ΔOD decay kinetics at gradually longer probe wavelengths approaching the observed isosbestic point of ~470 nm yielded time constants that were progressively smaller, which is consistent with the increase in the ΔOD spectrum in this spectral region due to concomitant Meta-I formation, but still within a reasonable experimental uncertainty of the ~48 μsec time constant estimate.

The Meta-I intermediate subsequently decays on the 100 μsec to 5 msec timescale, as shown in Fig. 5*C*, which results in the gradual formation of a significantly blue-shifted ΔOD band with its peak wavelength located at ~365 nm. We identify this transition process as the conversion of the Meta-I intermediate into the final, metastable Meta-II intermediate, which persisted for several hundreds of milliseconds following pulsed excitation. The corresponding isosbestic point for this transition is located at ~400 nm (Fig. 5*C*). In addition, the time constant for the Meta-II formation kinetics is estimated as ~0.6 msec, as displayed in Fig. 5*D*, based on the increase in the ~365 nm ΔOD band. The representative ΔOD spectra for the Lumi, Meta-I, and Meta-II photo-intermediates of human blue cone opsin are summarized in Fig. 6.

In addition to the differences in their respective ΔOD band maxima, the Lumi, Meta-I, and Meta-II photo-intermediate ΔOD spectra for human blue cone opsin clearly have distinct band shapes (Fig. 6). Particularly, the Meta-II intermediate displays the narrowest ΔOD bandwidth (FWHM), while the Lumi and Meta-I intermediates appear to have comparable, broader bandwidths. In the ΔOD spectrum of the Meta-II intermediate, we also observed a residual, nonzero tail in the ~475 to 550 nm spectral region that is directly adjacent to the ground-state bleach signal centered at ~420 nm. This general shape of the ΔOD spectrum for the Meta-II intermediate persisted for several hundreds of milliseconds following pulsed excitation. We attribute this residual, positive ΔOD band to Meta-I absorption, which suggests that the Meta-I intermediate is not fully converted to the Meta-II intermediate but rather undergoes only partial conversion. Consequently, we propose that the Meta-I and Meta-II intermediates are in dynamic equilibrium on these timescales, resulting in incomplete conversion of Meta-I into Meta-II.

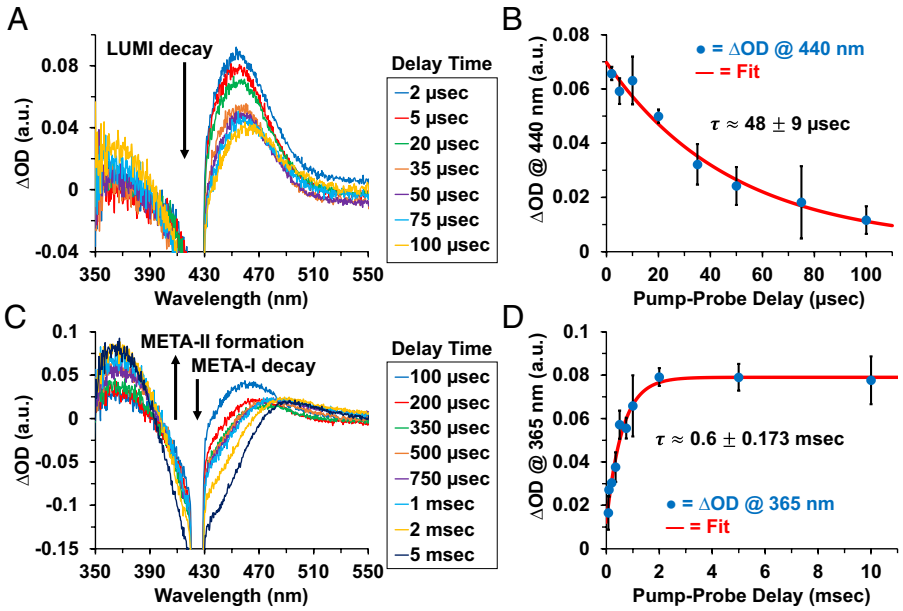

Fig. 5. Microsecond to millisecond transient absorption spectra and kinetics of human blue cone opsin. (*A*) Microsecond transient absorption spectra of human blue cone opsin, illustrating the decay of the Lumi-intermediate and formation of the Meta-I intermediate on the microsecond timescale. (*B*) Lumi to Meta-I transition kinetics recorded at a probe wavelength of ~440 nm. (*C*) Microsecond to millisecond transient absorption spectra of human blue cone opsin, illustrating the decay of the Meta-I intermediate and formation of the Meta-II intermediate on the millisecond timescale. (*D*) Meta-I to Meta-II transition kinetics recorded at a probe wavelength of ~365 nm. Note that for (*B*) and (*D*), each individual data point corresponds to the average ΔOD value computed across multiple pump laser shots at a given pump–probe delay time, and the error bars at each data point represent one SD from the mean.

Discussion

This study describes the ultrafast time-resolved absorption spectra and reaction kinetics of the major photo-intermediates formed following pulsed excitation of the human blue cone visual pigment at room temperature. Comparison of our blue cone spectral and kinetic data with our recent time-resolved studies (46, 56, 68) of bovine rhodopsin and human green cone opsin, as shown in Fig. 7, reveals several interesting similarities and differences in the mechanisms of rod and cone pigment activation.

In general, the basic sequence of major photo-intermediates is consistent among the studied rod and cone visual pigments, consisting of Batho, Lumi, Meta-I, and Meta-II intermediates that are progressively formed on the ultrafast, picoseconds or shorter (39), to millisecond timescales. Additionally, we find that the green cone and blue cone visual pigments exhibit the formation of a distinct BL-intermediate within a few nanoseconds after pulsed excitation, which is not observed with bovine rhodopsin over the same timescale (68). The BL-intermediate was initially detected in studies of chicken red cone opsin (62, 63), and our similar observations of this intermediate in both human green cone opsin and human blue cone opsin strongly imply that the BL-intermediate is a unique intermediate conserved across the cone visual pigments. Recent low-temperature UV-Vis and FTIR spectroscopic studies (75, 76) on primate blue cone opsin have demonstrated that the Batho to BL transition involves local, structural relaxation of both the all-*trans*-retinal chromophore and surrounding opsin protein. These structural changes, which are essentially localized to the chromophore binding pocket, occur due to the highly distorted all-*trans*-retinal configuration present in the Batho-intermediate (11, 75). The subsequent Lumi, Meta-I, and Meta-II photo-intermediates are then formed with progressively larger conformational changes (11, 19).

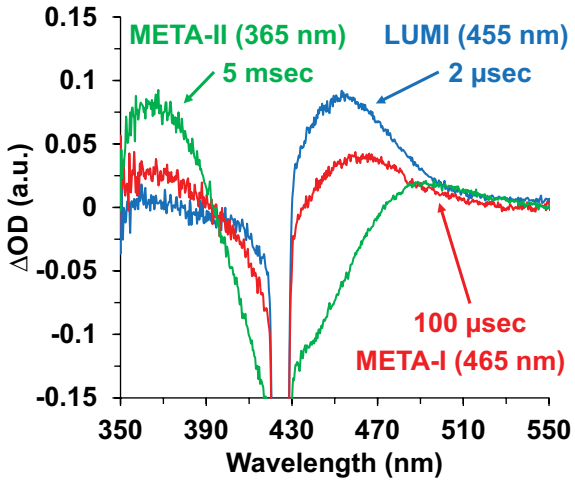

Fig. 6. Summary of the Lumi, Meta-I, and Meta-II photo-intermediate ΔOD spectra recorded for human blue cone opsin on the microsecond to millisecond timescales. The representative timescales and approximate ΔOD band maxima for each photo-intermediate are noted.

While the general mechanism of activation is similar among the studied rod and cone visual pigments, we find many unique spectral and kinetic characteristics for the human blue cone photo-intermediates (Fig. 7). In particular, the blue cone photo-intermediates, specifically those formed prior to the Meta-II intermediate, all appear highly overlapped in their respective ΔOD spectra and band maxima. Notably, the spectral redshift (relative to the corresponding ground-state absorption band maximum) of the Batho-intermediate ΔOD band maximum for blue cone opsin is only ~40 nm, which is considerably smaller than the ~70 nm and ~90 nm spectral redshifts for bovine rhodopsin and green cone opsin, respectively. The Batho to BL spectral shifts (in the corresponding ΔOD band maxima) for blue cone opsin and green cone opsin are relatively similar, ~10 to 20 nm, in magnitude. Additionally, the Batho/BL to Lumi spectral shift is merely ~25

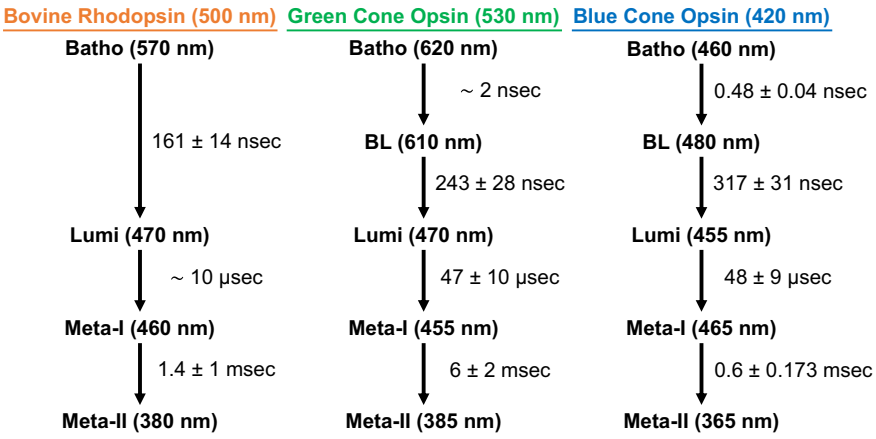

Fig. 7. Comparison of the photobleaching sequences for bovine rhodopsin, human green cone opsin, and human blue cone opsin. The approximate ground-state (steady-state) absorption band maximum and photo-intermediate ΔOD band maxima for each visual pigment are noted, along with the corresponding transition time constants. The spectral and kinetic data for bovine rhodopsin and human green cone opsin are based on our previous studies (46, 56, 68).

nm for blue cone opsin, whereas it is at least ~100 nm for bovine rhodopsin and green cone opsin. While the Lumi to Meta-I spectral shift is comparable (~10 to 15 nm) across all the studied rod and cone visual pigments, we find that the Meta-I to Meta-II spectral shift is the largest, ~100 nm, for blue cone opsin, which also exhibits the Meta-II intermediate with the shortest ΔOD band maximum at ~365 nm (Fig. 6). Thus, while the corresponding ΔOD band maxima of the initial Batho-intermediate and subsequent BL-intermediate appear to shift in accordance with the respective ground-state absorption maxima of the visual pigments, the ΔOD band maxima of the later Lumi, Meta-I, and Meta-II photo-intermediates are all located in similar spectral regions across the various visual pigments. Furthermore, we note that the specific directions of certain blue cone photo-intermediate spectral shifts appear to be unique, namely the recorded redshifts of the Batho to BL and Lumi to Meta-I transitions, where the equivalent transitions in bovine rhodopsin and human green cone opsin instead exhibit blueshifts in the ΔOD band maxima. These various spectral differences between the photo-intermediates of the rod and cone visual pigments are fundamentally due to the unique structures of the rod and cone opsin proteins (11, 19).

In addition to the unique photo-intermediate ΔOD spectra, the blue cone opsin photo-intermediate kinetics, starting with the decay of the initial Batho-intermediate, display several similarities and differences with the corresponding transition kinetics for bovine rhodopsin and human green cone opsin (Fig. 7). Notably, the Lumi-intermediate formation kinetics for blue cone opsin, ~317 nsec, are clearly the slowest (nearly by a factor of two relative to bovine rhodopsin), whereas the Lumi to Meta-I transition kinetics for green cone opsin and blue cone opsin are strikingly similar with associated time constants of ~48 µsec each that are larger by a factor of nearly five compared to bovine rhodopsin. In contrast to green cone opsin, however, we find that the Meta-I to Meta-II transition kinetics for blue cone opsin are essentially comparable (within the experimental error) with those for bovine rhodopsin, whereas the corresponding green cone opsin transition kinetics are substantially slower (nearly by an order of magnitude relative to blue cone opsin). Thus, the green cone opsin and blue cone opsin transition kinetics are rather similar up to the formation of the Meta-I intermediate, whereupon the subsequent Meta-II formation kinetics are considerably faster for both bovine rhodopsin and blue cone opsin.

A possible mechanism for the observed kinetic differences in Meta-II formation among bovine rhodopsin, green cone opsin, and blue cone opsin may involve the structural differences in the locations of the specific counterions that help stabilize the ground-state forms, namely the protonated Schiff base linkages, of each pigment, along with mediating the intramolecular proton transfer reaction that results in deprotonation of the Schiff base linkage during Meta-II formation (9, 11, 19, 77). Molecular modeling and dynamics simulations (78) indicated that the spatial locations of the counterions for bovine rhodopsin, E113 in transmembrane helix (TM) 3 and E181 in extracellular loop (ECL) 2 (19, 77, 79), are conserved in specifically human blue cone opsin, whereas the equivalent counterions in human green cone opsin and human red cone opsin are instead located in TM3 and TM2. Preliminary cryogenic electron microscopy structures (80) of the human cone visual pigments appear to corroborate these structural differences in the counterions. In addition, low-temperature spectroscopy of primate green cone opsin similarly implicated E102 in TM2 as a key residue mediating visual pigment activation (81). Hence, our time-resolved kinetic data (Fig. 7) strongly suggests that bovine rhodopsin and human blue cone opsin undergo similar conformational changes with comparable kinetics, which are highly distinct from those exhibited by human green cone opsin, during the Meta-I to Meta-II transition, thus demonstrating the critical role of the Schiff base counterions in determining the kinetics of Meta-II activation. In contrast to a recent low-temperature study (75) of primate blue cone opsin that suggests deprotonation of the retinal Schiff base may occur as early as the Lumi-intermediate, our time-resolved spectral data (Fig. 7) for human blue cone opsin is consistent with deprotonation occurring specifically during the Meta-I to Meta-II transition at room temperature, as commonly observed in vertebrate visual pigments (9, 19).

While the kinetics of the Meta-I to Meta-II transition are highly similar between bovine rhodopsin and blue cone opsin, we find that both green cone opsin and blue cone opsin exhibit the common characteristic of incomplete conversion of Meta-I into Meta-II, whereas bovine rhodopsin displays practically complete Meta-I to Meta-II conversion. This is evidenced by the residual Meta-I ΔOD bands displayed by both blue cone opsin (Fig. 6) and green cone opsin (68), but not bovine rhodopsin (46, 68), following Meta-II formation. Partial conversion of Meta-I into Meta-II was also previously observed with chicken red cone opsin following nanosecond laser photolysis (63). This apparent dynamic equilibrium and incomplete conversion between the Meta-I and Meta-II cone photo-intermediates strongly suggests that the Meta-I to Meta-II conversion efficiency is lower in the cone visual pigments relative to bovine rhodopsin under our experimental conditions. This is possibly due to the fact that cone visual pigments generally have significantly higher thermal instability (29,

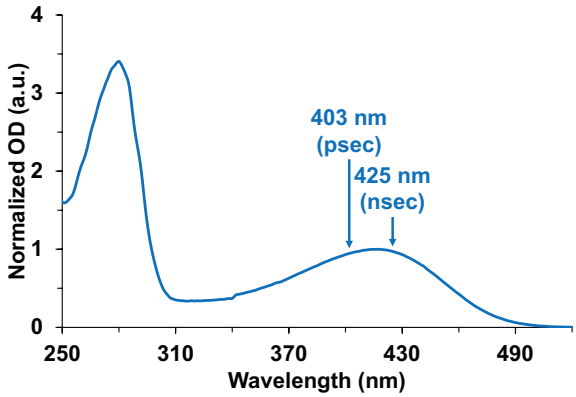

Fig. 8. Normalized steady-state absorption spectrum of human blue cone opsin solubilized in LMNG-buffer. The arrows designate the pump wavelengths employed in the ultrafast transient absorption experiments.

59), and hence considerably faster Meta-II decay rates (11, 34, 36, 37), which may explain the increased efficiency of the Meta-II to Meta-I reverse reaction in the human cone opsins compared to bovine rhodopsin. These properties of cone visual pigments, coupled with significantly faster rates of chromophore hydrolysis (74, 82) and subsequent pigment regeneration (11, 32, 83) relative to rhodopsin, enable cones to provide sustained vision under photopic conditions (3).

Conducting a similar time-resolved study of the human red cone visual pigment will allow us to make more definitive conclusions regarding the overall mechanism of cone pigment activation. While human blue cone opsin exhibits only ~43% amino acid sequence identity with each of the other human rod and cone opsins, the human green and red cone opsins share ~96% amino acid sequence identity (11, 84). Several site-directed mutagenesis studies (70–72, 85–89) have identified key amino acid residues that modulate the steady-state absorption spectra of rod and cone visual pigments (11, 22, 69, 90), and these residue differences might also explain the observed variation in the corresponding photo-intermediate spectra and kinetics (Fig. 7). On this basis, we expect that the photobleaching sequence of red cone opsin will share considerable similarity with that of green cone opsin.

Conclusion

We have recorded the ultrafast time-resolved absorption spectra and kinetics of the human blue cone visual pigment at room temperature on the picosecond to millisecond timescales. The general sequence of photo-intermediates formed was very similar to those of the bovine rhodopsin and human green cone opsin visual pigments, consisting of distinct Batho, BL, Lumi, Meta-I, and Meta-II photo-intermediates observed on progressively longer timescales following pulsed excitation. The transient spectra and transition kinetics of the blue cone photo-intermediates exhibited both similarities and differences with those of bovine rhodopsin and green cone opsin. In particular, the blue cone photo-intermediate bands were highly overlapped with considerably small spectral shifts. We also find that while the Meta-II formation kinetics between bovine rhodopsin and blue cone opsin are comparable, the qualitative features of the Meta-I to Meta-II transition are instead more similar between blue cone opsin and green cone opsin. These results suggest that while there are structural and kinetic characteristics of Meta-II activation common to bovine rhodopsin and blue cone opsin, functional differences between rod and cone visual pigments also impact the nature of the Meta-I to Meta-II transition. Additional time-resolved studies of human red cone opsin, along with other vertebrate cone visual pigments, will further elucidate the distinct mechanisms of rod and cone pigment activation.

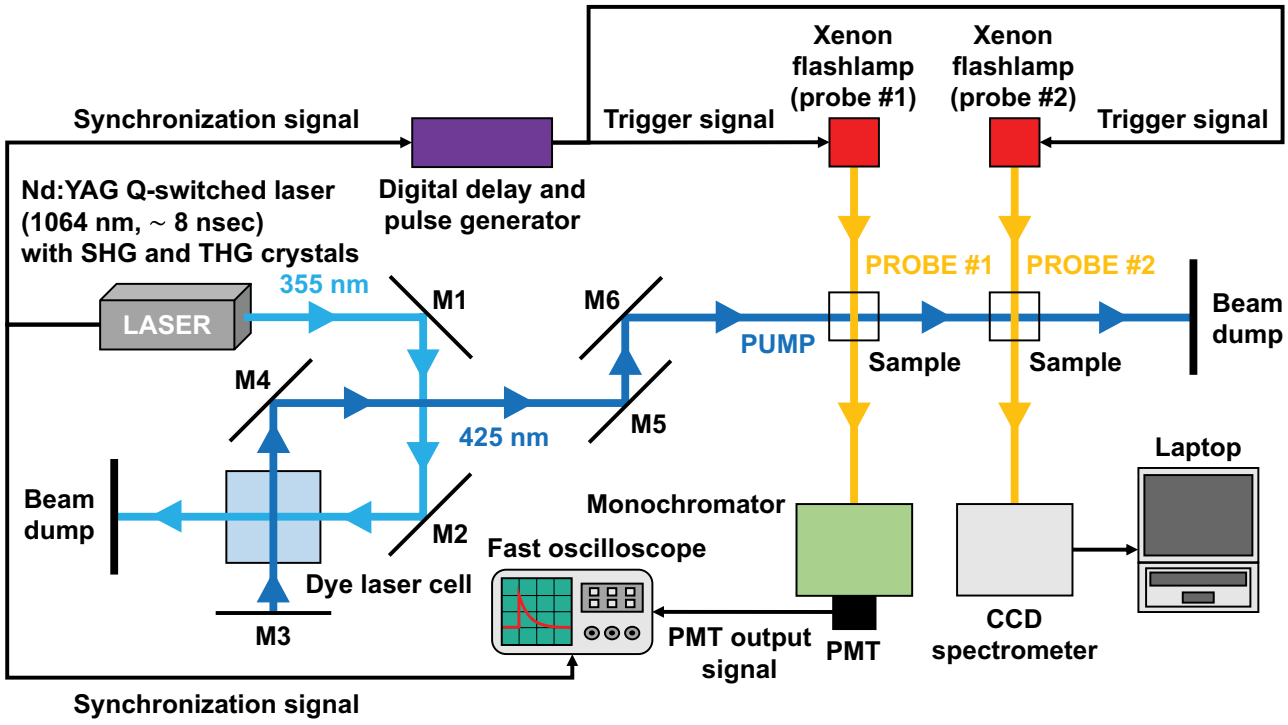

Fig. 9. Schematic diagram of the nanosecond transient absorption experimental system.

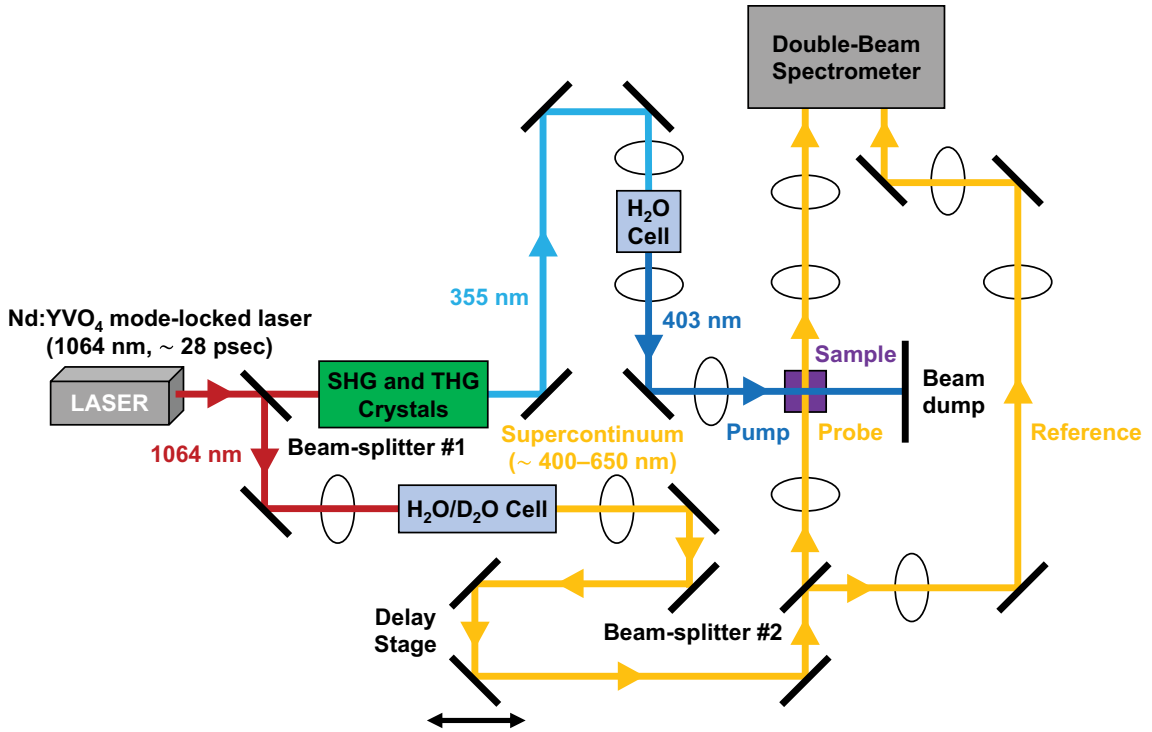

Fig. 10. Schematic diagram of the picosecond transient absorption experimental system.

Materials and Methods

Blue Cone Opsin Expression and Steady-State Absorption Measurements. Wild-type human blue cone opsin was generated recombinantly in Sf9 insect cells using similar procedures as described previously for human green cone opsin (58, 68) but without the insertion of a thermostabilizing fusion protein. The human blue cone opsin visual pigment was purified and solubilized in the detergent, lauryl maltose neopentyl glycol (LMNG), with buffer (50 mM HEPES pH 7.5 + 0.2 M NaCl + 0.2 mM LMNG) using similar procedures as detailed in (68). We note that the specific detergent used for solubilization can determine the observed kinetics of the Meta-II photo-intermediate in particular (91, 92), but it has practically no effect on the kinetics of the initial Batho to Lumi photo-intermediates (93). The human blue cone opsin concentration was ~0.8 to 1 mg/mL for the time-resolved experiments. All human blue cone opsin samples were kept frozen in the dark until use.

The steady-state absorption spectrum of human blue cone opsin was recorded with a Shimadzu 1601 UV-Vis spectrophotometer. All steady-state absorption measurements were performed at room temperature under dim red light. For the time-resolved experiments, the typical maximum optical density was ~0.75 to 1 a.u. (for a 10 mm path length) at the steady-state absorption band maximum (~420 nm) of the human blue cone opsin sample. The normalized steady-state absorption spectrum of human blue cone opsin is shown in Fig. 8.

Nanosecond Transient Absorption System and Experiments. Our nanosecond transient absorption experimental system, shown in Fig. 9, has been described previously (46, 56, 68). This system was modified to generate pump pulses at a wavelength suitable for the excitation of human blue cone opsin.

Briefly, the third harmonic, ~355 nm, output of a Q-switched Nd:YAG nanosecond laser (New Wave Research, Model: Tempest-20) was utilized, in conjunction with a stilbene 420 dye laser cell (1 cm quartz cuvette), to generate nanosecond pump pulses centered at ~425 nm with an ~5 nm spectral bandwidth (FWHM). The stilbene 420 dye concentration was ~0.3 mg/mL when dissolved in methanol. The stilbene dye laser pump pulses had a typical pulse energy of ~2 mJ/pulse with an ~8 nsec pulse width (FWHM). Two distinct Xenon flashlamp probes were employed for interrogation.

The first Xenon flashlamp probe (probe #1) emits a relatively broad, ~100 μsec (FWHM) in duration, pulse that is spatially overlapped with the ~425 nm pump pulse at the sample cell. Temporally, the ~4 μsec region of peak, essentially constant, flash intensity is synchronized, through a digital delay generator (Stanford Research Systems, Model: DG535), with the arrival of the pump pulse at the sample. The probe intensity, after transmission through the sample cell, is detected with a photomultiplier tube (Hamamatsu, Model: R928) that is situated at the output of a monochromator (Jarrell Ash, Model: 82-410) that enables the probe wavelength to be varied. The photomultiplier tube output voltage is recorded in time by a fast oscilloscope (Tektronix, Model: TDS3052B), with 50 ohm input impedance, that allows the ΔOD kinetic transient at a given probe wavelength to be computed based on the probe intensity before and after pumping the sample. Scanning the probe wavelength facilitates the recording of ΔOD spectra at various pump–probe delays. This probe was employed for pump–probe delays up to ~1 μsec.

The second Xenon flashlamp probe (probe #2) emits a relatively narrow, ~200 nsec (FWHM) in duration, pulse that is also spatially overlapped with the ~425 nm pump pulse at the sample cell. The relative time delay between the pump and probe pulses is controlled by a digital delay generator (Stanford Research Systems, Model: DG535). The broadband probe spectrum, after passing through the sample cell, is detected and recorded by a TE-cooled (~0 °C) CCD spectrometer (B&W Tek, Model: Exemplar Plus) that enables the ΔOD spectrum at a given pump–probe delay time to be computed based on the probe spectra with and without pumping the sample. Varying the pump–probe delay facilitates the recording of ΔOD kinetics at various probe wavelengths. This probe was employed for pump–probe delays varying from ~1 μsec to seconds.

For the nanosecond time-resolved experiments, the nanosecond pump laser was operated in the single-shot mode, and the blue cone opsin sample was placed in a 10 μL microchannel cuvette with a 1 mm pump path length and 10 mm probe path length. All nanosecond time-resolved measurements were conducted at room temperature under dim red light, and the sample aliquot was replaced with a fresh sample aliquot after each individual pump laser shot to minimize photobleaching effects.

Picosecond Transient Absorption System and Experiments. Our picosecond transient absorption experimental system, shown in Fig. 10, has been described previously (56, 68). This system was modified to generate pump pulses at a wavelength suitable for the excitation of human blue cone opsin.

Briefly, part of the fundamental, ~1,064 nm, output of a passively mode-locked Nd:YVO_4 picosecond laser (Ekspla, Model: PL2230) was utilized, in conjunction

with SHG and THG crystals, to generate the ~355 nm third harmonic that was subsequently focused into a 10 cm H_2O Raman laser cell to create stimulated Stokes Raman output centered at ~403 nm with an ~3 nm spectral bandwidth (FWHM). The picosecond Raman pump pulses at ~403 nm had a typical pulse energy of ~0.3 mJ/pulse and pulse width (FWHM) of ~28 psec.

The remaining part of the ~1,064 nm fundamental output is focused into a 20 cm H_2O/D_2O cell to create a broadband supercontinuum (~400 to 650 nm) that is subsequently divided into reference and probe beams. The reference beam is utilized for monitoring fluctuations in the probe supercontinuum, while the probe beam is focused and spatially overlapped with the ~403 nm pump beam at the sample cell. The precise temporal delay between the pump and probe pulses is controlled by means of a linear translation delay stage in the probe path. Both the probe and reference beams are directed into a double-beam spectrograph (Acton Research Corporation, Model: SpectraPro-150) that is integrated with a TE-cooled (~−75 °C) 2-D CCD camera (Princeton Instruments, Model: PIXIS:400). The probe and reference beam spots on the camera are each vertically binned to yield probe and reference spectra that are recorded with and without the pump pulse, thus enabling calculation of the corresponding ΔOD spectrum at a given pump–probe delay. By varying the pump–probe delay, the ΔOD kinetics at various probe wavelengths can be determined. With this experimental system, picosecond ΔOD spectra were recorded for pump–probe delays up to a few nanoseconds.

For the picosecond time-resolved experiments, the picosecond pump laser was operated in the single-shot mode, and the blue cone opsin sample was placed in a 10 μL microchannel cuvette with a 1 mm pump path length and 10 mm probe path length. Owing to the limited amount of fresh blue cone opsin sample available and the relatively low pump pulse energy at ~403 nm, multiple pump laser shots were conducted on each sample aliquot at a given pump–probe delay time for additional signal averaging. Specifically, each sample aliquot at a given pump–probe delay was gently stirred after every ~5 to 10 pump laser shots and replaced with a fresh sample aliquot after generally ~30 to 60 pump laser shots in total. In addition, a fresh sample aliquot was always used when varying the pump–probe delay. Under these experimental conditions, the ΔOD bands recorded for a sample aliquot at a given pump–probe delay persisted across several pump laser shots, at least the duration over which the aliquot was used, and displayed reasonable consistency in both the ΔOD band magnitude and shape for each pump laser shot that was averaged. All picosecond time-resolved measurements were conducted at room temperature under dim red light.

Data Analysis. For the picosecond time-resolved measurements (from picoseconds to nanoseconds), the ΔOD spectra at various pump–probe delays were computed using a custom-written MATLAB program based on the corresponding probe and reference spectra recorded with and without the pump pulse. The approximate "time zero" delay stage position, when the pump and probe pulses temporally overlap in the sample cell, was experimentally determined and utilized to calculate the corresponding set of pump–probe delay times. Computation of the picosecond ΔOD kinetics at a given probe wavelength was performed in MATLAB with the Curve Fitting Toolbox.

For the nanosecond time-resolved measurements with probe #1 (from nanoseconds to microseconds), the set of ΔOD transients at all detected probe wavelengths were computed based on the corresponding probe intensities before and after the pump pulse at time zero. Subsequently, the exponential fittings (one-term or two-term, depending on the specific probe wavelength) of the transient ΔOD kinetics at each probe wavelength were performed in MATLAB with the Curve Fitting Toolbox. The computed set of ΔOD kinetic exponential fits, across the range of scanned probe wavelengths, were then utilized to determine the corresponding fitted transient ΔOD spectra at various pump–probe delay times.

For the nanosecond time-resolved measurements with probe #2 (from microseconds to seconds), the recorded probe spectra, with and without the pump pulse, were utilized directly in the BWSpec (B&W Tek) software to derive the corresponding ΔOD spectrum at a given pump–probe delay time. Computation of the microsecond to millisecond ΔOD kinetics at a given probe wavelength was similarly performed in MATLAB with the Curve Fitting Toolbox.

Data, Materials, and Software Availability. All study data are included in the main text.

ACKNOWLEDGMENTS. This study was supported in part by the Air Force Office of Scientific Research (AFOSR) under Grant No. FA9550-20-1-0139 and by Texas A&M Engineering Experiment Station (TEES) funds. This research was supported in part by NIH research Grants EY034519 and EY09339 (NEI) to K.P. We acknowledge support from a Research to Prevent Blindness Unrestricted Grant to the Department of Ophthalmology at UCI.

1. V. Y. Arshavsky, Like night and day: Rods and cones have different pigment regeneration pathways. *Neuron* **36**, 1–3 (2002).
2. Y. Fu, K.-W. Yau, Phototransduction in mouse rods and cones. *Pflügers Archiv-Eur. J. Physiol.* **454**, 805–819 (2007).
3. S. Kawamura, S. Tachibanaki, Molecular bases of rod and cone differences. *Prog. Retin. Eye Res.* **90**, 101040 (2022).
4. D.-G. Luo, T. Xue, K.-W. Yau, How vision begins: An odyssey. *Proc. Natl. Acad. Sci. U.S.A.* **105**, 9855–9862 (2008).
5. T. Ebrey, Y. Koutalos, Vertebrate photoreceptors. *Prog. Retin. Eye Res.* **20**, 49–94 (2001).
6. D. Mustafi, A. H. Engel, K. Palczewski, Structure of cone photoreceptors. *Prog. Retin. Eye Res.* **28**, 289–302 (2009).
7. D. A. Baylor, T. D. Lamb, K.-W. Yau, Responses of retinal rods to single photons. *J. Physiol.* **288**, 613–634 (1979).
8. F. Rieke, D. A. Baylor, Single-photon detection by rod cells of the retina. *Rev. Modern Phys.* **70**, 1027 (1998).
9. Y. Shichida, T. Matsuyama, Evolution of opsins and phototransduction. *Philos. Trans. R Soc. Lond. B Biol. Sci.* **364**, 2881–2895, (2009).
10. K. W. Yau, R. C. Hardie, Phototransduction motifs and variations. *Cell* **139**, 246–264 (2009).
11. Y. Imamoto, Y. Shichida, Cone visual pigments. *Biochim. Biophys. Acta* **1837**, 664–673 (2014).
12. G. H. Jacobs, Photopigments and the dimensionality of animal color vision. *Neurosci. Biobehav. Rev.* **86**, 108–130 (2018).
13. M. H. Rowe, Trichromatic color vision in primates. *Physiology* **17**, 93–98 (2002).
14. W. B. Thoreson, D. M. Dacey, Diverse cell types, circuits, and mechanisms for color vision in the vertebrate retina. *Physiol. Rev.* **99**, 1527–1573 (2019).
15. J. K. McBee, K. Palczewski, W. Baehr, D. R. Pepperberg, Confronting complexity: The interlink of phototransduction and retinoid metabolism in the vertebrate retina. *Progr. Retinal Eye Res.* **20**, 469–529 (2001).
16. B. M. Kevany, K. Palczewski, Phagocytosis of retinal rod and cone photoreceptors. *Physiol. (Bethesda)* **25**, 8–15 (2010).
17. A. Terakita, The opsins. *Genome Biol.* **6**, 1–9 (2005).
18. K. Palczewski, G protein–coupled receptor rhodopsin. *Annu. Rev. Biochem.* **75**, 743–767 (2006).
19. O. P. Ernst *et al.*, Microbial and animal rhodopsins: Structures, functions, and molecular mechanisms. *Chem. Rev.* **114**, 126–163 (2014).
20. S. Filipek, R. E. Stenkamp, D. C. Teller, K. Palczewski, G protein-coupled receptor rhodopsin: A prospectus. *Annu. Rev. Physiol.* **65**, 851–879 (2003).
21. S. Gulati, K. Palczewski, Structural view of G protein–coupled receptor signaling in the retinal rod outer segment. *Trends Biochem. Sci.* **48**, 172–186 (2023).
22. J. F. D. Hagen, N. S. Roberts, R. J. Johnston Jr., The evolutionary history and spectral tuning of vertebrate visual opsins. *Dev. Biol.* **493**, 40–66 (2023).
23. J. C. Corbo, Vitamin A(1)/A(2) chromophore exchange: Its role in spectral tuning and visual plasticity. *Dev. Biol.* **475**, 145–155 (2021).
24. T. Baden, D. Osorio, The retinal basis of vertebrate color vision. *Annu. Rev. Vis. Sci.* **5**, 177–200 (2019).
25. A. Wand, I. Gdor, J. Zhu, M. Sheves, S. Ruhman, Shedding new light on retinal protein photochemistry. *Annu. Rev. Phys. Chem.* **64**, 437–458 (2013).
26. R. R. Birge, Nature of the primary photochemical events in rhodopsin and bacteriorhodopsin. *Biochimica et Biophysica Acta (BBA)-Bioenergetics*, **1016**, 293–327 (1990).
27. J. W. Lewis, D. S. Kliger, Photointermediates of visual pigments. *J. Bioenerget. Biomembranes* **24**, 201–210 (1992).
28. H. Kandori, Y. Shichida, T. Yoshizawa, Photoisomerization in rhodopsin. *Biochemistry (Moscow)* **66**, 1197–1209 (2001).
29. Y. Shichida, H. Imai, Visual pigment: G-protein-coupled receptor for light signals. *Cell. Mol. Life Sci. CMLS* **54**, 1299–1315 (1998).
30. J. D. Hong, K. Palczewski, A short story on how chromophore is hydrolyzed from rhodopsin for recycling. *Bioessays* **45**, e2300068 (2023).
31. D. C. A. Barret, U. B. Kaupp, J. Marino, The structure of cyclic nucleotide-gated channels in rod and cone photoreceptors. *Trends Neurosci.* **45**, 763–776 (2022).
32. S. Kawamura, S. Tachibanaki, Explaining the functional differences of rods versus cones. *Wiley Interdiscip. Rev.: Membr. Transport Signaling* **1**, 675–683 (2012).
33. K. Sato, T. Yamashita, Y. Imamoto, Y. Shichida, Comparative studies on the late bleaching processes of four kinds of cone visual pigments and rod visual pigment. *Biochemistry* **51**, 4300–4308 (2012).
34. Y. Imamoto, I. Seki, T. Yamashita, Y. Shichida, Efficiencies of activation of transducin by cone and rod visual pigments. *Biochemistry* **52**, 3010–3018 (2013).
35. H. Imai *et al.*, Single amino acid residue as a functional determinant of rod and cone visual pigments. *Proc. Natl. Acad. Sci. U.S.A.* **94**, 2322–2326 (1997).
36. Y. Shichida, H. Imai, Y. Imamoto, Y. Fukada, T. Yoshizawa, Is chicken green-sensitive cone visual pigment a rhodopsin-like pigment? A comparative study of the molecular properties between chicken green and rhodopsin *Biochemistry* **33**, 9040–9044 (1994).
37. H. Imai, Y. Imamoto, T. Yoshizawa, Y. Shichida, Difference in molecular properties between chicken green and rhodopsin as related to the functional difference between cone and rod photoreceptor cells. *Biochemistry* **34**, 10525–10531 (1995).
38. T. Gruhl *et al.*, Ultrafast structural changes direct the first molecular events of vision. *Nature* **615**, 939–944 (2023).

39. M. A. Ostrovsky, V. A. Nadtochenko, Femtochemistry of rhodopsins. *Russian J. Phys. Chem. B* **15**, 344–351 (2021).
40. T. B. Feldman *et al.*, Femtosecond spectroscopic study of photochromic reactions of bacteriorhodopsin and visual rhodopsin. *J. Photochem. Photobiol. B* **164**, 296–305 (2016).
41. M. N. Sandberg *et al.*, Low-temperature trapping of photointermediates of the rhodopsin E181Q mutant. *SOJ biochemistry* **1**, 12 (2014).
42. T. Yoshizawa, G. Wald, Pre-lumirhodopsin and the bleaching of visual pigments. *Nature* **197**, 1279–1286 (1963).
43. K. Peters, M. Applebury, P. Rentzepis, Primary photochemical event in vision: Proton translocation. *Proc. Natl. Acad. Sci. U.S.A.* **74**, 3119–3123 (1977).
44. R. G. Matthews, R. Hubbard, P. K. Brown, G. Wald, Tautomeric forms of metarhodopsin. *J. General Physiol.* **47**, 215–240 (1963).
45. T. E. Thorgeirsson, J. W. Lewis, S. E. Wallace-Williams, D. S. Kliger, Effects of temperature on rhodopsin photointermediates from lumirhodopsin to metarhodopsin II. *Biochemistry* **32**, 13861–13872 (1993).
46. D. Dhankhar *et al.*, Comparison of bovine and carp fish visual pigment photo-intermediates at room temperature. *Photochem. Photobiol.* **98**, 1303–1311 (2022).
47. O. A. Smitienko *et al.*, Femtosecond formation dynamics of primary photoproducts of visual pigment rhodopsin. *Biochemistry (Mosc)* **75**, 25–35 (2010).
48. G. Busch, M. Applebury, A. Lamola, P. Rentzepis, Formation and decay of prelumirhodopsin at room temperatures. *Proc. Natl. Acad. Sci. U.S.A.* **69**, 2802–2806 (1972).
49. V. Sundstrom, P. Rentzepis, K. Peters, M. Applebury, Kinetics of rhodopsin at room temperature measured by picosecond spectroscopy. *Nature* **267**, 645–646 (1977).
50. R. Bensasson, E. J. Land, T. Truscott, *Laser Flash Photolysis of Rhodopsin at Room Temperature* (Wiley Online Library, 1977), pp. 601–605.
51. Y. G. Thomas, I. Szundi, J. W. Lewis, D. S. Kliger, Microsecond time-resolved circular dichroism of rhodopsin photointermediates. *Biochemistry* **48**, 12283–12289 (2009).
52. R. Bensasson, E. J. Land, T. Truscott, Nanosecond flash photolysis of rhodopsin. *Nature* **258**, 768–770 (1975).
53. J. Horwitz, J. Lewis, M. Powers, D. Kliger, Nanosecond laser photolysis of rhodopsin and isorhodopsin. *Photochem. Photobiol.* **37**, 181–188 (1983).
54. R. W. Schoenlein, L. A. Peteanu, R. A. Mathies, C. V. Shank, The first step in vision: Femtosecond isomerization of rhodopsin. *Science* **254**, 412–415 (1991).
55. P. Kukura, D. W. McCamant, S. Yoon, D. B. Wandschneider, R. A. Mathies, Structural observation of the primary isomerization in vision with femtosecond-stimulated Raman. *Science* **310**, 1006–1009 (2005).
56. A. Krishnamoorthi, K. Khosh Abady, D. Dhankhar, P. M. Rentzepis, Ultrafast transient absorption spectra and kinetics of rod and cone visual pigments. *Molecules* **28**, 5829 (2023).
57. A. Wu *et al.*, Structural basis for the allosteric modulation of rhodopsin by nanobody binding to its extracellular domain. *Nat. Commun.* **14**, 5209 (2023).
58. T. S. Owen, D. Salom, W. Sun, K. Palczewski, Increasing the stability of recombinant human green cone pigment. *Biochemistry* **57**, 1022–1030 (2018).
59. E. Ramon, X. Mao, K. D. Ridge, Studies on the stability of the human cone visual pigments. *Photochem. Photobiol.* **85**, 509–516 (2009).
60. V. L. Mooney, I. Szundi, J. W. Lewis, E. C. Yan, D. S. Kliger, Schiff base protonation changes in Siberian hamster ultraviolet cone pigment photointermediates. *Biochemistry* **51**, 2630–2637 (2012).
61. J. Liang, R. Govindjee, T. G. Ebrey, Metarhodopsin intermediates of the gecko cone pigment P521. *Biochemistry* **32**, 14187–14193 (1993).
62. T. Yoshizawa, Y. Imamoto, Structure and photobleaching process of chicken iodopsin. *Biophys. Chem.* **56**, 57–62 (1995).
63. Y. Shichida, T. Okada, H. Kandori, Y. Fukada, T. Yoshizawa, Nanosecond laser photolysis of iodopsin, a chicken red-sensitive cone visual pigment. *Biochemistry* **32**, 10832–10838 (1993).
64. H. Kandori *et al.*, Bathoiodopsin, a primary intermediate of iodopsin at physiological temperature. *Proc. Natl. Acad. Sci. U.S.A.* **87**, 8908–8912 (1990).
65. T. Yoshizawa, O. Kuwata, Iodopsin, a red-sensitive cone visual pigment in the chicken retina. *Photochem. Photobiol.* **54**, 1061–1070 (1991).
66. J. W. Lewis, I. Szundi, M. A. Kazmi, T. P. Sakmar, D. S. Kliger, Time-resolved photointermediate changes in rhodopsin glutamic acid 181 mutants. *Biochemistry* **43**, 12614–12621 (2004).
67. S. J. Hug, J. W. Lewis, C. M. Einterz, T. E. Thorgeirsson, D. S. Kliger, Nanosecond photolysis of rhodopsin: Evidence for a new blue-shifted intermediate. *Biochemistry* **29**, 1475–1485 (1990).
68. D. Dhankhar, D. Salom, K. Palczewski, P. M. Rentzepis, Ultrafast spectra and kinetics of human green-cone visual pigment at room temperature. *Proc. Natl. Acad. Sci. U.S.A.* **120**, e2214276120 (2023).
69. J. K. Bowmaker, Evolution of vertebrate visual pigments. *Vision Res.* **48**, 2022–2041 (2008).
70. S. W. Lin *et al.*, Mechanisms of spectral tuning in blue cone visual pigments. Visible and raman spectroscopy of blue-shifted rhodopsin mutants. *J. Biol. Chem.* **273**, 24583–24591 (1998).
71. J. I. Fasick, N. Lee, D. D. Oprian, Spectral tuning in the human blue cone pigment. *Biochemistry* **38**, 11593–11596 (1999).
72. J. I. Fasick, M. L. Applebury, D. D. Oprian, Spectral tuning in the mammalian short-wavelength sensitive cone pigments. *Biochemistry* **41**, 6860–6865 (2002).
73. H. Imai *et al.*, Photochemical and biochemical properties of chicken blue-sensitive cone visual pigment. *Biochemistry* **36**, 12773–12779 (1997).
74. J. D. Hong *et al.*, Retinylidene chromophore hydrolysis from mammalian visual and non-visual opsins. *J. Biol. Chem.* **300**, 105678 (2024).
75. Y. Mizuno, K. Katayama, H. Imai, H. Kandori, Early proton transfer reaction in a primate blue-sensitive visual pigment. *Biochemistry* **61**, 2698–2708 (2022).
76. S. Hanai, K. Katayama, H. Imai, H. Kandori, Light-induced difference FTIR spectroscopy of primate blue-sensitive visual pigment at 163 K. *Biophys. Physicobiol.* **18**, 40–49 (2021).
77. K. Tsutsui, Y. Shichida, Multiple functions of Schiff base counterion in rhodopsins. *Photochem. Photobiol. Sci.* **9**, 1426–1434 (2010).
78. S. Srinivasan *et al.*, Human blue cone opsin regeneration involves secondary retinal binding with analog specificity. *Biophys. J.* **114**, 1285–1294 (2018).
79. S. O. Smith, Mechanism of activation of the visual receptor rhodopsin. *Annu. Rev. Biophys.* **52**, 301–317 (2023).
80. Q. Peng *et al.* Cryo-EM structures of human cone visual pigments. bioRxiv [Preprint] (2024). https://doi.org/10.1101/2024.01.30.577689 (Accessed 3 June 2024).
81. T. Sasaki, K. Katayama, H. Imai, H. Kandori, Glu102(2.53)-Mediated early conformational changes in the process of light-induced green cone pigment activation. *Biochemistry* **63**, 843–854 (2024).
82. J. D. Hong *et al.*, Chromophore hydrolysis and release from photoactivated rhodopsin in native membranes. *Proc. Natl. Acad. Sci. U.S.A.* **119**, e2213911119 (2022).
83. J. S. Wang, V. J. Kefalov, The cone-specific visual cycle. *Prog. Retin. Eye Res.* **30**, 115–128 (2011).
84. J. Nathans, D. Thomas, D. S. Hogness, Molecular genetics of human color vision: The genes encoding blue, green, and red pigments. *Science* **232**, 193–202 (1986).
85. K. J. Fujimoto *et al.*, Molecular mechanism of spectral tuning by chloride binding in monkey green sensitive visual pigment. *J. Phys. Chem. Lett.* **14**, 1784–1793 (2023).
86. A. B. Asenjo, J. Rim, D. D. Oprian, Molecular determinants of human red/green color discrimination. *Neuron* **12**, 1131–1138 (1994).
87. S. L. Merbs, J. Nathans, Role of hydroxyl-bearing amino acids in differentially tuning the absorption spectra of the human red and green cone pigments. *Photochem. Photobiol.* **58**, 706–710 (1993).
88. J. Nathans, Determinants of visual pigment absorbance: Role of charged amino acids in the putative transmembrane segments. *Biochemistry* **29**, 937–942 (1990).
89. T. Nakayama, H. G. Khorana, Mapping of the amino acids in membrane-embedded helices that interact with the retinal chromophore in bovine rhodopsin. *J. Biol. Chem.* **266**, 4269–4275 (1991).
90. S. Yokoyama, Molecular evolution of vertebrate visual pigments. *Prog. Retin. Eye Res.* **19**, 385–419 (2000).
91. B. König, W. Welte, K. P. Hofmann, Photoactivation of rhodopsin and interaction with transducin in detergent micelles: Effect of 'doping'with steroid molecules. *FEBS Lett.* **257**, 163–166 (1989).
92. H. Tsukamoto, I. Szundi, J. W. Lewis, D. L. Farrens, D. S. Kliger, Rhodopsin in nanodiscs has native membrane-like photointermediates. *Biochemistry* **50**, 5086–5091 (2011).
93. J. Epps, J. W. Lewis, I. Szundi, D. S. Kliger, Lumi I→ Lumi II: The last detergent independent process in rhodopsin photoexcitation. *Photochem. Photobiol.* **82**, 1436–1441 (2006).